Graphene formation on metal surfaces investigated by *in-situ* scanning tunneling microscopy

New Journal of Physics

Graphene formation on metal surfaces investigated by *in-situ* scanning tunneling microscopy

G C Dong, D W van Baarle, M J Rost and J W M Frenken[1]

Kamerlingh Onnes Laboratory, Leiden University, PO Box 9504,
2300 RA Leiden, The Netherlands
E-mail: frenken@physics.leidenuniv.nl

Abstract. Hydrocarbon decomposition on transition metals provides a practical way of producing graphene. Here, ethylene deposition on Rh (111) is taken as an example. *In-situ* scanning tunneling microscopy measurements, under various growth conditions and at temperatures up to 1100 K, were carried out, revealing the processes of graphene formation at the atomic level. The initial nucleation stage nearly completely determines the phase in which further C is deposited, graphene or rhodium carbide, and the orientation of the growing graphene patches. We demonstrate that by separating the stages of nucleation and further growth and controlling other growth parameters, we obtain graphene of higher quality, while avoiding carbide formation and controlling the dissolved C to form graphene. Based on these observations, a universal physical picture emerges for graphene formation on metal surfaces.

S Online supplementary data available from stacks.iop.org/NJP/14/053033/mmedia

---

[1] Author to whom any correspondence should be addressed.

IOP Institute of Physics **ⅅ** DEUTSCHE PHYSIKALISCHE GESELLSCHAFT

Contents

1. Introduction

Graphene, a single layer of graphite, has drawn much attention in recent years, because of its special properties and its potential applications, for example, in future-generation electronics [1, 2]. However, reproducibly manufacturing high-quality graphene has remained a challenge. To date, most of the high-quality graphene, for example, for use in experiments requiring high carrier mobilities, is still obtained from graphite by the 'scotch-tape' method [3]. Most of the methods for assembling graphene directly result in material with a high defect density, caused by multilayer growth [4, 5] or chemical contamination [6]. These imperfections seriously influence the properties and stability of graphene.

Chemical vapor deposition (CVD) of hydrocarbons on transition metals (TMs) provides a practical method for the production of graphene [4, 7–14]. Since newly arriving hydrocarbon molecules do not stick to or decompose on graphene, CVD may lead to the formation of precisely a single graphene layer when dissolution and segregation of C can be ignored. However, one can also exploit the temperature-dependent solubility of C in TMs to produce graphene from segregated C [7, 10, 13, 15, 16]. Usually, after samples are prepared at high temperature, the structure and properties of the resulting graphene are only inspected afterwards, at, or even below, room temperature. In those cases, it is unclear which kind of C, segregated or deposited, forms the graphene layer. Nevertheless, using this method, some reliable and reproducible recipes have been developed for the production of graphene [4, 5, 16, 17], even though the growth mechanism is still not very clear. Many previous experiments on graphene growth have focused on finding suitable growth conditions and only a smaller number on understanding the precise mechanisms at work [7, 10, 18–20], even though this may prove essential for improving the quality of grown graphene. The graphene formation process occurs at elevated temperatures. If measurements are carried out at room temperature or lower after sample preparation, it is difficult to guess the reaction path, especially in cases where graphene has formed during cooling down of the sample. Real space, *in-situ* experiments at the atomic level are required for revealing this information.

Our scanning tunneling microscope (STM) allows fast scanning while changing the temperature and measuring at high temperatures [21, 22], offering the possibility of following the reaction and growth of graphene *in situ*. Our example of ethylene on Rh(111) covers the full complexity of C on TMs, resulting in carbide formation [23], C dissolution [24] or graphene

formation [25]. This manifold of possibilities makes it suitable for a universal demonstration. The threefold (111) orientation was chosen to work as a template for graphene crystallization. In addition, graphene forms a moiré pattern on Rh(111). A simple calculation shows that the moiré pattern exaggerates ('magnifies') the translational and rotational defects in the graphene layer. For example, $1°$ of actual graphene rotation with respect to the Rh lattice results in a $10°$ apparent rotation in the moiré pattern. In this way, atomic information of graphene can be obtained, without actually achieving atomic resolution with the STM. In this paper, detailed observations are made of ethylene on the Rh(111) system, from which we derive the conditions for the formation and stability of graphene and carbide. These conditions are not limited to the conventional parameters of temperature and pressure, but also concern the near-surface concentration profile of dissolved C, which depends on the full history of the Rh crystal. Armed with this information, we will demonstrate how to avoid carbide formation and how to control the dissolved C to form graphene, and we will attempt to derive the optimal recipe for graphene growth. The combination of our observations results in a universal physical picture of graphene formation on metal surfaces. Using this picture, we will explain all our results as well as some of the graphene formation results achieved by other groups. Based on this simple picture it becomes, in principle, straightforward to control the balance between different C phases and improve the quality of graphene also in other systems.

2. Experimental setup

All measurements were carried out in an ultrahigh vacuum (UHV) system with a variable-temperature STM (prototype of the commercial VT-STM of Leiden Probe Microscopy BV). The UHV system was further equipped with standard surface-science instruments, including low-energy electron diffraction (LEED), Auger electron spectroscopy (AES) and a differentially pumped, focused ion gun for sputter cleaning. The base pressure of the system was 4×10^{-11} mbar. Sample temperatures were measured by a K-type thermocouple, spot-welded directly onto the Rh single crystal. The size of the Rh(111) sample was $1 \times 4.8 \times 4.8$ mm^3. The Rh sample was cleaned by cycles of Ar$^+$ ion sputtering, followed by flash annealing to 1300 K and exposure of the sample to 2–3×10^{-7} mbar of O$_2$ for 1–2 h at temperatures of 700–800 K. Residual O was removed from the Rh surface by flashing the sample to 1000 K [24].

3. Temperature dependence of graphene and carbide formation

The experiment started with the deposition of ethylene on clean Rh(111) at room temperature. Following deposition, the sample was slowly heated up, while the surface was imaged with the STM. At room temperature, ethylene was adsorbed on the surface up to its saturation coverage, causing the rough appearance of the Rh, as shown by figure 1(A); this image was obtained after exposure to 3×10^{-5} mbar of ethylene at room temperature. While this pre-covered surface was heated up, clusters formed without any edge orientation preference (figure 1(B)). These clusters grew in size when the temperature was increased. Even though we have directly observed the motion and coalescence of the clusters, the drifting during temperature changes makes it difficult to conclude that this was the sole ripening mechanism. It is known from earlier work that ethylene decomposition on Rh proceeds in several stages between room temperature and ∼800 K [25, 26]. So the irregular structures in figure 1(B) are probably clusters of CH$_x$ or C atoms. At temperatures around 870 K, some islands acquired a hexagonal shape and a
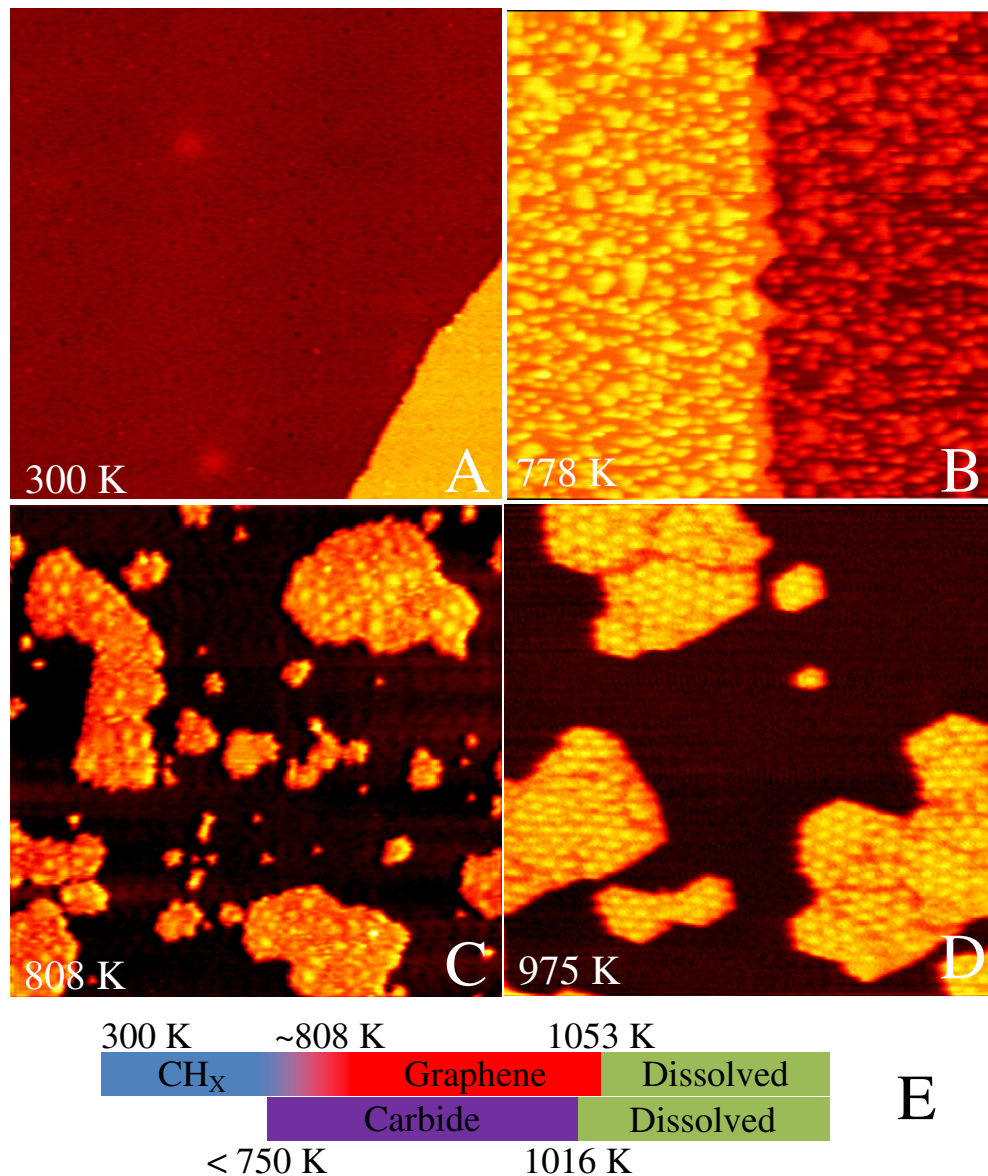
Figure 1. STM images measured during continuous heating from 300 K to ~1000 K, after room temperature ethylene deposition. Panels (A), (B) and (D) are from one series of experiments. (A) The Rh(111) surface, directly after exposure to 3×10^{-5} mbar of ethylene at room temperature. A mono-atomic step on the Rh surface crosses the image. The saturated ethylene adsorption layer causes the rough appearance. (B) At 778 K, the overlayer is organized into irregular clusters, but no moiré pattern was found at this temperature. (C) Starting from 4×10^{-7} mbar of ethylene deposition at room temperature, this image shows the lowest temperature where the moiré pattern of graphene was found. (D) At 975 K, the graphene ripened into larger islands with similar orientations. (E) Sketch of the temperature ranges for the formation and dissolution of graphene and carbide on the Rh surface. All STM images are 85 nm × 85 nm, and they have been taken at sample voltages of $V_b = 0.05$, 1.16, 1.43 and -1.84 V for panels (A)–(D), respectively, and at a tunneling current of $I_t = 0.05$ nA.

moiré pattern. This indicates that, at these temperatures, graphene had already formed, and the domains were large enough to appear as moiré patterns. Of course, the graphene layer must have started with small domains of graphene too small to appear as a moiré pattern. Only for those domains that had grown in size beyond the lattice period of the moiré pattern, via some ripening process, had this pattern become visible in the STM images. Because any ripening process requires the relocation of many C atoms, this ripening should be relatively slow [27]. The combination of this slow ripening with the fast temperature ramp up to 870 K of $0.2 \, K \, s^{-1}$ implies that the moiré pattern observed at 870 K is a sign that graphene formation had started already at a temperature below 870 K. Indeed, figure 1(C) shows that the lowest temperature at which we could find the moiré pattern was 808 K (the temperature ramp rate was $0.05 \, K \, s^{-1}$). This is close to the 700–800 K range for which ethylene decomposition is known to be complete [25, 26]. Up to 969 K, the ripening of the graphene islands continued, and the islands became more compact, bigger and with a more prominent hexagonal shape (figure 1(D)). During this process, the differences in orientation angle between different domains became smaller. This suggests that certain orientations were energetically more favorable than others and these ripened at the expense of the others. Actually, we found more than one type of moiré pattern at this high temperature, which means that some configurations may have similarly low energies. In any case, the Rh(111) substrate has an influence on the orientation of the graphene formed. Finally, in a similar but separate experiment we found that the graphene layer dissolved into the Rh substrate when we raised the temperature to 1053 K. We summarize the C phases observed during this heating experiment in the form of the upper temperature bar in figure 1(E).

From the first experiment, it was seen that, from 808 to 1053 K, graphene can be found on the Rh(111) surface. This 250 K temperature range for stable graphene on Rh is much wider than the 50 K window that has been reported previously [28]. This process, combining adsorption of ethylene at room temperature with a subsequent temperature ramp, also yields a lower graphene formation temperature than the temperature of ~1100 K, reported in the case where ethylene was dosed directly at high temperature [29]. We will return to these differences in temperature later in this paper. Similar to the nanomesh structure of *h*-BN on Rh(111) [30], the defects in the graphene layer are caused by two classes of domain boundaries. When two nuclei with different orientations grow out and merge, a defect line in the graphene will be formed between them. It will contain point defects, such as 5-rings, 7-rings [11] and possibly even dangling bonds. Even if the nuclei have precisely the same orientation, there are still more than 200 possibilities for the choice of the origin of the superstructure, which reduces the chances of their fitting perfectly to a negligible value, below 0.5%. There will then be a phase defect line in the moiré pattern. We speculate that this phase defect is not leading to dangling bonds, i.e. the defect is present only in the period and the superstructure but not in the topology of the graphene network [11]. In both cases, well-oriented and mis-oriented domains, the defect density is fully determined by the nucleation density. To reduce the density of domain boundaries by encouraging the diffusion of the C atoms, we exposed a clean Rh sample directly to ethylene at an elevated temperature of 830 K. As predicted by nucleation theory [31], this should result in a lower nucleation density. With our STM, it was seen that an overlayer formed, starting from the steps on the Rh(111) surface, and that it covered the whole surface in a step-flow manner. Unfortunately, this overlayer appeared to be different from graphene, as can be seen in figure 2(A). After this layer had covered the entire surface, the sample was heated to higher temperature. The layer did not transform into graphene up to
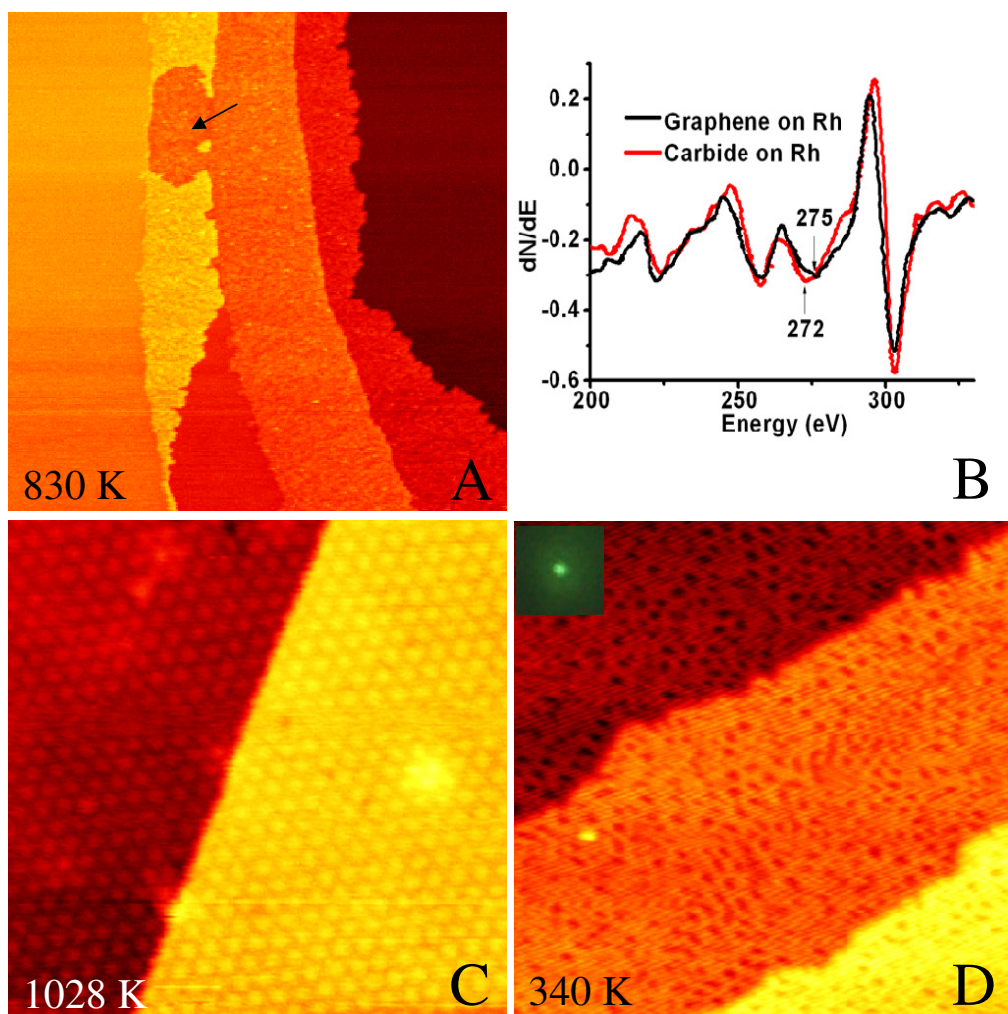
Figure 2. Direct ethylene deposition on Rh(111) at different temperatures. (A) An STM image measured at 830 K, during ethylene deposition. A rough carbide layer started developing from step edges of the Rh. Before nucleation began, the Rh steps were modified, as indicated by the arrow. Nucleation started when the ethylene pressure reached 4.4×10^{-8} mbar. (B) The Auger spectrum of an Rh surface covered by a carbide monolayer, which was obtained by ethylene deposition at 750 K. For comparison the AES spectrum is shown for an Rh surface covered by a single monolayer of graphene. (C) An STM image of graphene-covered Rh, which was achieved by direct ethylene deposition and imaging at 1028 K. The pressure of ethylene was 3.9×10^{-6} mbar. (D) An STM image of the sample of (C), after it was cooled to 340 K. The moiré pattern of graphene was deformed. The inset in (D) shows one integer-order Rh LEED spot (the same view as in the inset of figure 3(B)) and the near absence of superstructure spots around it, recorded at room temperature. All images are 65 nm × 65 nm, and they have been taken at sample voltages of $V_b = 2.79$, 4.83 and 3.74 V for panels (A), (C) and (D), respectively, and at a tunneling current of $I_t = 0.05$ nA.

a temperature of 1016 K, at which we observed that it dissolved into the Rh substrate. The different temperature of dissolution indicates that this overlayer was neither graphene nor the CH_x cluster structure mentioned above. A similar structure was also found when ethylene was deposited on a clean Rh surface at 750 K. AES (figure 2(B)) on this layer shows that the KLL of C peak had shifted from 272 to 275 eV and the MNN peak of Rh had also undergone a change in shape and position. Both shifts indicate the formation of a new compound [32]. We suggest that this is a rhodium carbide overlayer. Comparing this AES spectrum with a reference spectrum taken on a one-monolayer graphene-covered Rh surface (figure 2(B)), we see that the C-to-Rh peak ratios for these two cases were similar. Assuming that the Rh peak in the AES spectrum of graphene-covered Rh corresponds to effectively one atomic layer of Rh, we find that the C-to-Rh ratio in the carbide must have been of the order of 2 : 1. The formation and stability of the carbide layer are summarized in the lower temperature bar in figure 1(E). Attempts were also made to deposit ethylene directly onto Rh at an even higher temperature, e.g. 982 K. Here we observed regions similar to figure 2(C) and other regions similar to figure 2(A), i.e. both graphene and carbide were present on the surface. According to the two temperature bars in figure 1(E), this should not be surprising: at 982 K, both carbide and graphene can be formed. Note that there is also a narrow temperature window, between 1016 and 1053 K, at which carbide is not stable but graphene is. In order to explore this window, we exposed the Rh to ethylene at 1028 K. Indeed, at this temperature, a graphene layer was observed to cover the whole surface and to be well aligned with the Rh substrate (misalignment between graphene and Rh below 1°; figure 2(C)) at the deposition temperature. After this successful deposition, we monitored the graphene layer with the STM during the slow cooling down. To our surprise, we found that the moiré pattern of graphene became distorted, as shown in figure 2(D). The LEED pattern that was taken afterwards at room temperature showed a weak Rh(111) pattern on a strong, diffuse background (the inset of figure 2(D)). We suggest that this distortion was caused by C that had first dissolved into the Rh at the growth temperature and segregated back to the surface when the temperature was decreased. It is well known that C can dissolve into Rh at elevated temperatures and that part of the dissolved C accumulates at the surface upon cooling [24]. In the experiment of figure 2(D), this segregated C may have led to the nucleation of islands of a second graphene or carbide layer, between the original one and the Rh substrate.

4. The crucial role of the history of the sample

From this set of experiments, it was found that the temperature window for preparing graphene by direct deposition is quite limited, and graphene formed at this temperature distorts when the temperature is reduced to room temperature. On the other hand, the first experiment, which started with deposition at room temperature, showed a wider temperature window for graphene formation (upper bar in figure 1(E)), which starts below and ends above the carbide window (lower bar in figure 1(E)). This lower onset temperature will be associated with less C dissolution and, if it is of any importance, also with a lower strain due to the differential thermal expansion between the graphene overlayer and the Rh substrate [33, 34]. The differences between the two experiments in figures 1 and 2(A) further suggest that the choice made by the growing overlayer between carbide and graphene, in the temperature interval from 800 to 1016 K, was fully determined by the structure of the early overlayer nuclei; in other words, graphene patches always continued to grow as graphene, whereas carbide patches always

continued to grow as carbide. In turn, this suggests a refinement of our approach, by separating the stages of nucleation and further growth. We could start with the graphene-seeded Rh surface from the first experiment and expose that to further ethylene under different conditions to obtain full coverage by graphene. We may expect nucleation and growth of the graphene overlayer to follow well-known rules, in which the nucleation density is determined by F/D, where F is the flux of arriving atoms and D is their surface diffusion coefficient [31]. If the deposition is carried out very slowly, so that the number determined by F/D is smaller than the existing seed density on the surface, the newly arriving C atoms should all be incorporated into the edges of growing graphene islands, thus preventing them from forming their own nuclei [35]. There will then be no carbide, but only graphene, on the surface. The presence of the graphene seeds on the surface should have the additional effect that newly arriving C atoms have a strongly reduced probability of dissolving into the Rh, again because they will be incorporated into the graphene overlayer on a much shorter timescale, due to the difference in the rate of diffusion of the C atoms into the bulk and over the surface, which is expected to be significant. On a non-seeded surface, dissolution has to compete only with the rather rare processes of nucleation of either graphene or carbide. How 'difficult' graphene nucleation is on a hot Rh surface is evidenced by our following finding in a separate experiment on a clean Rh surface: we found that at 1028 K an ethylene pressure of up to 3.5×10^{-7} mbar was required for observing the first graphene nuclei in our STM images.

The suggested approach to ethylene deposition at high temperatures on an Rh surface that is pre-seeded with graphene by low-temperature deposition was successful. Figure 3 shows the result obtained at a growth temperature of 975 K; even more informative is the corresponding STM movie[2]. Starting with the end situation of the first experiment (figure 1(D)), ethylene was deposited, at a pressure of 3×10^{-9} mbar, which was increased at the end of the procedure to 3.4×10^{-8} mbar, simply to accelerate the process. The newly arrived C continued the structure and orientation of the graphene that was already present until the entire surface was covered by graphene. When a new kink formed at a concave corner between two differently oriented domains, it exhibited a preference to follow the graphene domain with the orientation closest to that of the Rh substrate. This preference was observed directly in the STM movie, in which the better-aligned graphene domain could always be distinguished easily, because it generates the moiré pattern with the larger period. In this way, the metal substrate guided the orientation of the graphene layer, which made the final density of domain boundaries lower than that expected from the initial configuration of graphene seeds. After the graphene overlayer was completed and had been cooled down subsequently to room temperature, neither the STM images nor the LEED pattern (insert of figure 3(B)) showed a degradation of the moiré pattern. The six superstructure spots that are clearly present around the integer-order maxima from the Rh in the LEED pattern indicated that the graphene layer had a preferred orientation; otherwise a ring of intensity should have been observed, rather than spots. Although the superstructure spots are not very sharp, the orientation differences between graphene domains must have been minor, because the moiré pattern exaggerates all variations in position and orientation, roughly by a factor of 10. The bright regions indicated by black arrows in figure 3(B) were formed in the final stage of the deposition. They will be explained below.
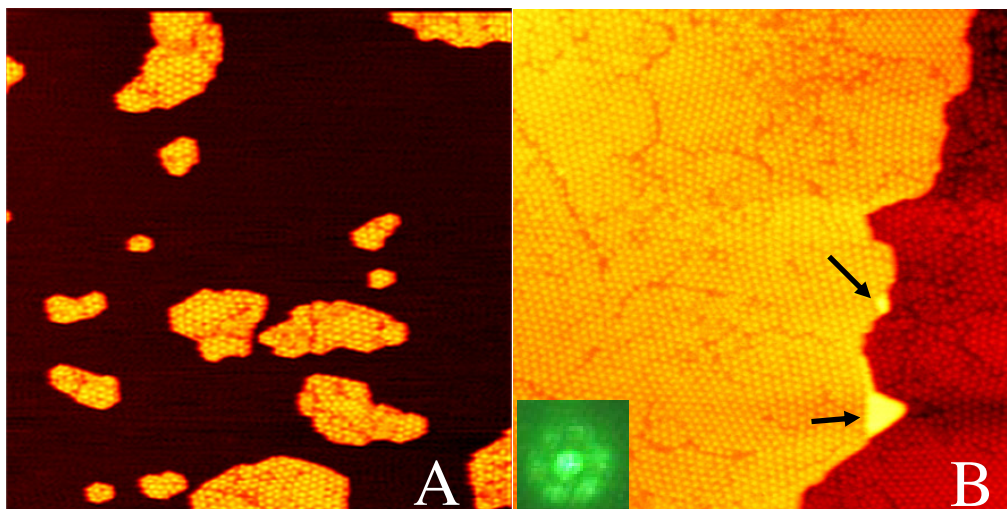
Figure 3. Graphene formation, starting with a seeded surface. (A) A graphene-seeded Rh surface, achieved by annealing a pre-exposed Rh(111) surface from room temperature to 975 K. Most of the graphene islands had the same orientation, as can be derived from the similarity of their moiré patterns. But superstructure domain boundaries can still be observed within most islands. (B) Graphene-covered Rh, after deposition of ethylene on the seeded surface at a temperature of 975 K and at pressures ranging from 3×10^{-9} to 3.4×10^{-8} mbar over 76 min. The domain boundary density became ~30% lower than that in the starting situation. Two Rh double-layer defects are indicated by the arrows. The inset of (B) shows the superstructure spots around one integer-order Rh LEED spot, obtained after the sample was cooled down to room temperature. The STM images are 160 nm × 160 nm and have been taken at a sample voltage of $V_b = -1.84$ V and a tunneling current of $I_t = 0.05$ nA.

5. Using segregated C to form graphene

In the above experiment, the conditions had been controlled such that exposure to ethylene led to the growth of graphene at a relatively low temperature instead of the formation of rhodium carbide. As an alternative to deposition, controlled segregation of dissolved C atoms was also used to grow graphene. By cooling down the sample very slowly, the effective flux of C segregating to the surface can be kept low enough to prevent the formation of new nuclei of either graphene or carbide. Once at the surface, also these C atoms are 'forced' to follow the structure and orientation of the pre-existing seeds, thus enabling us to manipulate the growth by again seeding the surface exclusively with graphene. This alternative procedure was successful, as is shown in figure 4(A), where a region on the surface was followed from 862 to 829 K. This is very promising for achieving two-dimensional (2D) single-crystalline graphene using dissolved C. One difference, relative to deposited C, is that the graphene layer also chose the growth direction (figure 4(E)), where the Rh step has to retract, to allow further graphene growth. This mechanism resembles the graphene growth by step etching reported on Ru(0001) [36]. To emphasize that this proceeds against the direction of regular step-flow growth, we refer to this as 'anti-step flow'. In this temperature regime, Rh atoms should be expected to diffuse
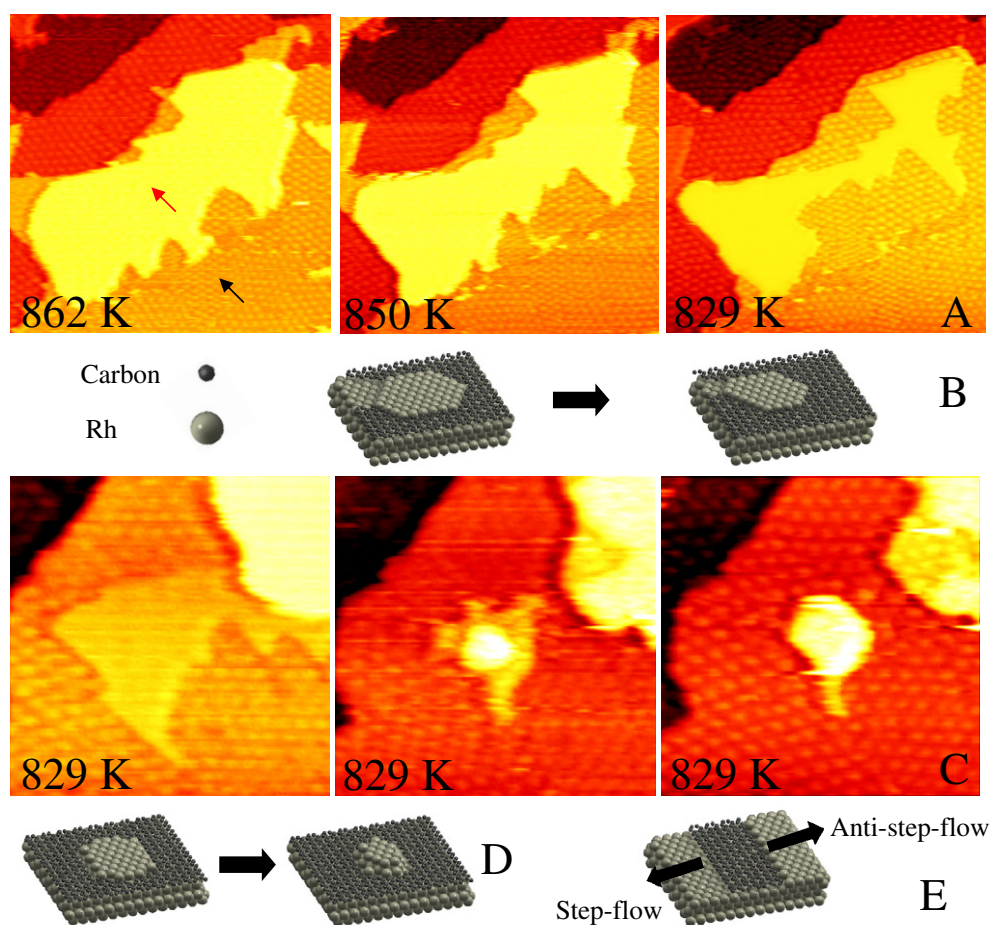
Figure 4. Graphene formation from segregated C and Rh double-layer defect formation. (A) STM images of the same area, acquired while a partially graphene-covered Rh(111) surface was cooled down, after adsorption of ethylene at room temperature and annealing to 977 K. The single-monolayer Rh island indicated by the red arrow is partially surrounded by the graphene that is indicated by the black arrow. The apparent height difference is an electronic effect and depends on the tunneling voltage. The C that segregated during the cool-down increased the graphene area, respecting the orientation of the graphene that was already present. Image size: $100 \times 100 \, nm^2$. (B) Ball model of the graphene growth ('anti-step-flow') process by segregated C. The Rh island could shrink, because Rh was allowed to diffuse away via a narrow passage in the surrounding graphene layer. (C) Graphene growth by exposure to more ethylene, while the sample was held at 829 K. These images show an Rh island, enclosed by graphene, being pushed into a double-layer island, with half of the original area. The growth of graphene stopped after the whole island had become two layers high. Image size: $50 \times 50 \, nm^2$. (D) Sketch of the formation of the Rh double-layer island. (E) Concept of 'step-flow' and 'anti-step-flow' growth of graphene. In the latter case, Rh atoms have to move out of the way, either to the upper atomic level or to another location along the metal step, in order to make room for the additional C.

much faster over the surface than the C atoms can in graphene. When sites become temporarily available, as a result of step fluctuations of the Rh, newly arriving C atoms may fill up the vacant sites, the strong cohesion in the graphene preventing the Rh step from fluctuating completely back to its original shape and location. We found that this anti-step-flow mechanism resulted in a large number of Rh islands enclosed by graphene. Figure 4(C) shows one of them, to which more ethylene had been added. The C introduced by the ethylene exposure was also found to be accommodated via the anti-step-flow mechanism, instead of forming graphene on top of the enclosed Rh. At this stage, Rh atoms were pushed up and nucleated a higher atomic layer; the graphene stopped growing when the complete enclosed Rh island had a double-layer height (figures 4(C) and (D)). The reason that in figure 4(A) the Rh did not become a double-layer structure is that in that case there was a narrow passage in the graphene layer, through which the Rh could diffuse away. In separate experiments in which we exposed the Rh to ethylene at a low temperature of 864 K, we observed growth of graphene both at the free edge of graphene islands ('step-flow' growth) and growth against the Rh steps ('anti-step-flow'). At this temperature, the growth speeds for these two mechanisms were comparable. At the higher temperatures of the experiments discussed earlier, e.g. at 975 K, the anti-step-flow growth rate was much lower than the step-flow growth rate. That the mechanism was still active is illustrated by the appearance of double-layer defects in the final stages of the graphene growth, as is indicated by the two arrows in figure 3(B). We explain the temperature dependence of the ratio between the two growth rates as follows. We assume that decomposition of ethylene or the growth of graphene has a lower energy barrier at the step edges of Rh than on the terraces. At 864 K, the resulting higher ethylene decomposition or graphene growth rate at the Rh steps makes the amount of C available for anti-step-flow higher than that for step-flow growth. At 975 K, all ethylene on the Rh terraces rapidly decomposes, which means that the C production rate is not limited at that temperature by the decomposition, but by the ethylene deposition. Since the steps represent a much smaller effective area than the terraces and the anti-step-flow requires an additional process of moving Rh atoms, the ratio between anti-step-flow and step-flow should become low at high temperatures. Nevertheless, anti-step-flow will still occur, and this will lead to Rh double-layer defects. The only way to reduce their density is by further elevating the temperature or by making the average distance between the graphene nuclei larger than the average distance between the steps on the Rh substrate.

6. A universal physical picture of graphene formation on transition metals

Inspired by the work of McCarty *et al* [10], we introduce a new physical picture (figure 5), based on our direct STM observations. In figure 5, the black line represents the adatom C density, dictated by equilibrium with C dissolved in the substrate. The shape and position of this line are determined by the C concentration in the bulk, and by the dissolution energy of C [10]. The solid red line represents the adatom density deriving from equilibrium with the graphene islands on the surface. The point where the black line crosses the solid red line gives the dissolution temperature of graphene. We now add the solid blue line, which represents the C adatom density that would establish equilibrium with carbide islands. We have drawn it higher than the red line for graphene because we observed a lower dissolution temperature for the carbide at a comparable C concentration in the bulk. The dashed red and blue lines indicate our generic estimates for the C adatom supersaturation values necessary for observable nucleation of graphene and carbide. The reason why we have drawn the dashed blue line (carbide) lower than
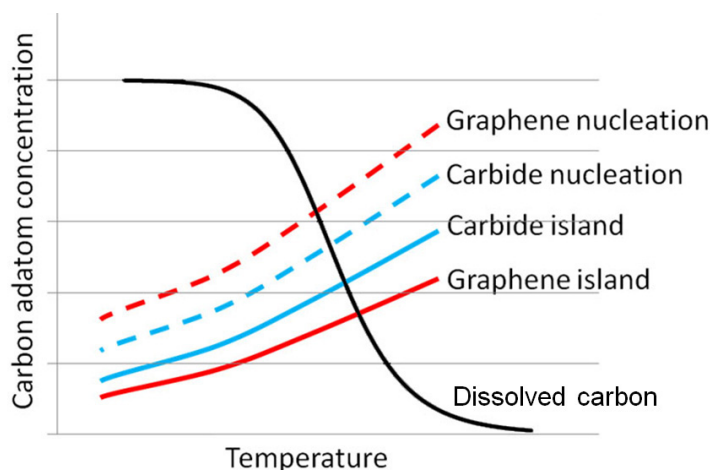
Figure 5. Schematic diagram showing the temperature dependence of various equilibrium adatom concentrations of C on the metal surface. Black line: C adatom concentration in equilibrium with dissolved, near-surface C (after McCarty *et al* [10]). Solid red line: adatom concentration in equilibrium with graphene islands (after McCarty *et al* [10]). Solid blue line: adatom concentration in equilibrium with carbide islands; locations where the two solid colored lines cross the black line are the dissolution temperatures for graphene and carbide. Dashed red and blue lines indicate the supersaturation levels required for nucleation of graphene and carbide, respectively, on a clean metal surface.

the dashed red line (graphene) is because of our observation that direct deposition of ethylene between 750 and 975 K leads to the carbide phase. A simple reason for this could be that the critical nucleus size for graphene is larger, for example, as a result of the dominating influence of the moiré structure.

Now let us see how this simple picture explains the full complexity of our observations. The diagram of figure 5 shows that when we exposed the sample to ethylene at 1028 K, carbide could not be formed, because at these high temperatures it would rather have dissolved. So under these conditions, graphene should be formed, accompanied by the dissolution of some C below the surface. This is in accordance with the observations in figures 2(C) and (D). In that experiment, the pressure of ethylene was raised to 3.9×10^{-6} mbar as rapidly as possible, in order to encourage the nucleation of graphene while minimizing the amount of dissolving C. Nevertheless, some C had necessarily dissolved into the bulk before the graphene nucleated, which had increased the C concentration near the surface. Upon cooling down, part of this C segregated to the Rh–graphene interface, distorting the overlayer and the associated moiré pattern. The diagram suggests that it should be possible to re-dissolve this segregated excess C by heating the sample to a temperature similar to the deposition temperature. We have performed such experiments and have indeed observed that the quality of the moiré pattern was restored when the sample was brought to a high temperature again. Since the dissolved C atoms increase the sub-surface C concentration, in this experiment an increase should be observed in the dissolution temperature of the graphene. This was indeed the case: the film in figure 2(C) was observed to dissolve at a temperature as high as 1118 K, i.e. well above the dissolution temperature of 1053 K observed in the experiment of figure 1, as indicated in figure 1(E). In

the experiments where the surface was first exposed to ethylene at room temperature and then warmed up, the clustering of CH_x must have locally made the surface C concentration very high, beyond the concentrations shown by the dashed blue and red lines in the diagram of figure 5, so that both carbide and graphene nuclei could be formed. With time, the carbide islands will disappear and the graphene islands will become bigger, as they are energetically more favorable. This is also the reason why the carbide may form first on metal surfaces, but after long periods of annealing (e.g. 400 min) at high temperature, it can transform into graphene [36]. In addition, ripening [27] has been active in making the average size of the graphene islands continue to grow. When ethylene was deposited on the graphene-seeded surface, as shown in figure 3, the system was kinetically trapped in a 'graphene-forming' mode. Only a low C adatom density was then needed to continue the growth. Because of the low ethylene pressure and the rapid incorporation of the deposited C into the graphene matrix, the density of adatoms was not high enough for nucleation of carbide (or new graphene islands). This situation resulted in a surface fully covered by graphene.

How to control the thickness of the graphene, i.e. how to avoid the nucleation of the second layer below the first layer, now seems evident: after the (first) graphene layer has been formed on the metal surface, the nucleation of a second layer can be avoided by cooling down the sample very rapidly. Also by choosing a metal with a low solubility for C, for example, Cu, nucleation of the second layer can be further suppressed. The two-step recipe, first nucleation and then growth, can be used to trap the system into a state with a lower amount of dissolved C in the metal substrate as demonstrated in this paper. This recipe is also useful in arriving at a low growth temperature at which a minimum of C dissolves in the substrate and the graphene overlayer grows with a low strain level. In the case of Rh, this recipe still resulted in a considerable density of translational defects, due to the relatively small domain size, but on other substrates, such as Ni(111), where there is no superstructure [38], we expect that this will not pose a problem.

Figure 5 shows that in order to have less C dissolved during the direct deposition, one should use a higher pressure. The argument for this counterintuitive approach is that when the pressure is raised, the nucleation rate increases super-linearly, whereas the rate of dissolution will simply be proportional to the pressure. Indeed, when ethylene exposure was performed at a low pressure, e.g. 1×10^{-8} mbar, some features were observed even before graphene started forming, which could be related to dissolved C. These were absent at the relatively high pressure of 3.9×10^{-6} mbar of figure 2(C). Nevertheless, in spite of the high ethylene pressure used here, the moiré pattern still distorted afterwards due to segregated C when the sample was cooled to room temperature (figure 2(D)). The combination of the high solubility of C in Rh and the macroscopic thickness of our substrate (1 mm) made it nearly impossible to avoid C dissolution at high temperatures and segregation of dissolved C during the cool-down.

One of the recipes reported for a single monolayer of graphene on Rh(111) is to expose the clean rhodium surface for 3 min to 2×10^{-7} mbar of ethylene at an even higher temperature of 1100 K [29]. We have monitored this recipe with our STM at this high temperature, but graphene was *not* formed under these conditions and also not with longer exploring times up to 10 min. Instead, our images show that in this case a graphene layer was formed only *after* the exposure, during cooling of the sample, when the temperature had reduced to ~1000 K, showing that, in this recipe, the graphene film is assembled completely from segregated C. The STM images at room temperature did not show distortions, in accordance with the images in Wang *et al* [29]. We attribute this absence of distortions to a nearly complete consumption of the dissolved C

IOP Institute of Physics Φ DEUTSCHE PHYSIKALISCHE GESELLSCHAFT

in the near-surface region by the graphene monolayer. The difficulty of this procedure lies in precisely controlling the coverage, i.e. the total amount of segregated C. It is relatively easy to obtain large areas covered by graphene suitable for STM imaging or for a local spectroscopic measurement. But it is very difficult to reach full coverage of the surface with graphene of precisely one layer thickness, i.e. without any excess C.

In conclusion, the schematic diagram in figure 5 explains all our experimental results. It is a generic diagram that can be adapted easily to other CVD procedures for graphene growth on Rh(111) and other TMs. The key elements that may vary from system to system are the precise stable phases, their formation energies and step energies, their dissolution energies and diffusion energies and their critical nucleation sizes. Figure 5 also naturally explains why the reported recipes sometimes appear difficult to reproduce. For example, the C adatom density at the surface is a function of the bulk C concentration in the near-surface region. The latter depends on the full history of the substrate, including the ethylene pressures to which the substrate was exposed, the time that the sample was held at elevated temperature, and the rate of increase or decrease of the temperature. These parameters vary from case to case and in publications they are often not specified.

7. Conclusion

The central message of this paper is that by following an appropriate path through the diagram in figure 5, one can control the nucleation, growth and transformations of the three C phases: graphene, carbide and dissolved C. Recipes for graphene production on a metal substrate should therefore not only consider the temperature and gas pressure as essential control parameters, but also the rates of temperature increase or decrease, the bulk and near-surface C concentrations of the metal substrate, dictated by the starting material and the full preparation and exposure history of the substrate, and the bulk diffusion coefficient of the dissolved C.

Acknowledgment

References

[1] Westervelt R M 2008 Applied physics—graphene nanoelectronics *Science* **320** 324–5
[2] Castro Neto A H *et al* 2009 The electronic properties of graphene *Rev. Mod. Phys.* **81** 109–62
[3] Du X *et al* 2009 Fractional quantum Hall effect and insulating phase of Dirac electrons in graphene *Nature* **462** 192–5
[4] Kim K S *et al* 2009 Large-scale pattern growth of graphene films for stretchable transparent electrodes *Nature* **457** 706–10
[5] Reina A *et al* 2009 Large area, few-layer graphene films on arbitrary substrates by chemical vapor deposition *Nano Lett.* **9** 30–5
[6] Guo H L *et al* 2009 A green approach to the synthesis of graphene nanosheets *ACS Nano* **3** 2653–9
[7] Loginova E *et al* 2009 Factors influencing graphene growth on metal surfaces *New J. Phys.* **11** 063046
[8] Martoccia D *et al* 2008 Graphene on Ru(0001): a 25 × 25 supercell *Phys. Rev. Lett.* **101** 126102
[9] Oshima C *et al* 2000 A heteroepitaxial multi-atomic-layer system of graphene and h-BN *Surf. Rev. Lett.* **7** 521–5

[10] McCarty K F *et al* 2009 Kinetics and thermodynamics of carbon segregation and graphene growth on Ru(0001) *Carbon* **47** 1806–13

[11] Coraux J *et al* 2008 Structural coherency of graphene on Ir(111) *Nano Lett.* **8** 565–70

[12] Oshima C and Nagashima A 1997 Ultra-thin epitaxial films of graphite and hexagonal boron nitride on solid surfaces *J. Phys.: Condens. Matter* **9** 1–20

[13] Sutter P W, Flege J I and Sutter E A 2008 Epitaxial graphene on ruthenium *Nature Mater.* **7** 406–11

[14] Wintterlin J and Bocquet M L 2009 Graphene on metal surfaces *Surf. Sci.* **603** 1841–52

[15] Isett L C and Blakely J M 1976 Segregation isosteres for carbon at (100) surface of nickel *Surf. Sci.* **58** 397–414

[16] Yu Q K *et al* 2008 Graphene segregated on Ni surfaces and transferred to insulators *Appl. Phys. Lett.* **93** 113103

[17] Sutter P 2009 Epitaxial graphene: how silicon leaves the scene *Nature Mater.* **8** 171–2

[18] Loginova E *et al* 2008 Evidence for graphene growth by C cluster attachment *New J. Phys.* **10** 093026

[19] Rut'kov E V and Gall N R 2009 Role of edge atoms of graphene islands on metals in nucleation, growth, alkali metal intercalation *Phys. Solid State* **51** 1738–43

[20] Wang B *et al* 2011 Size-selective carbon nanoclusters as precursors to the growth of epitaxial graphene *Nano Lett.* **11** 424–30

[21] Hoogeman M S *et al* 1998 Design and performance of a programmable-temperature scanning tunneling microscope *Rev. Sci. Instrum.* **69** 2072–80

[22] Rost M J *et al* 2005 Scanning probe microscopes go video rate and beyond *Rev. Sci. Instrum.* **76** 053710

[23] Chen J G *et al* 1998 Controlling surface reactivities of transition metals by carbide formation *J. Mol. Catal. A* **131** 285–99

[24] Delouise L A and Winograd N 1984 Carbon-monoxide adsorption and desorption on Rh(111) and Rh(331) surfaces *Surf. Sci.* **138** 417–31

[25] Castner D G, Sexton B A and Somorjai G A 1978 Leed and thermal desorption studies of small molecules (H$_2$, O$_2$, Co, Co$_2$, No, C$_2$H$_4$, C$_2$H$_2$ and C) chemisorbed on rhodium (111) and (100) surfaces *Surf. Sci.* **71** 519–40

[26] Dubois L H, Castner D G and Somorjai G A 1980 The chemisorption of acetylene and ethylene on Rh(111): A low energy electron diffraction (LEED), high resolution electron energy loss (ELS), and thermal desorption mass spectrometry (TDS) study *J. Chem. Phys.* **72** 5234–40

[27] Ibach H 2006 *Physics of Surfaces and Interfaces* vol 10 (Jülich: Springer) p 525

[28] Rut'kov E V, Kuz'michev A V and Gall N R 2011 Carbon interaction with rhodium surface: adsorption, dissolution, segregation, growth of graphene layers *Phys. Solid State* **53** 1092–8

[29] Wang B *et al* 2010 Coupling epitaxy, chemical bonding, and work function at the local scale in transition metal-supported graphene *ACS Nano* **4** 5773–82

[30] Dong G C *et al* 2010 How boron nitride forms a regular nanomesh on Rh(111) *Phys. Rev. Lett.* **104** 096102

[31] Venables J A 2001 *Introduction to Surface and Thin Film Processes* (Cambridge: Cambridge University Press)

[32] Sinharoy S and Levenson L L 1978 The formation and decomposition of nickel carbide in evaporated nickel films on graphite *Thin Solid Films* **53** 31–6

[33] Röhrl J *et al* 2008 Raman spectra of epitaxial graphene on SiC(0001) *Appl. Phys. Lett.* **92** 201918

[34] Zakharchenko K V, Katsnelson M I and Fasolino A 2009 Finite temperature lattice properties of graphene beyond the quasiharmonic approximation *Phys. Rev. Lett.* **102** 046808

[35] van Gastel R *et al* 2009 Selecting a single orientation for millimeter sized graphene sheets *Appl. Phys. Lett.* **95** 121901

[36] Starodub E *et al* 2009 Graphene growth by metal etching on Ru(0001) *Phys. Rev.* B **80** 235422

[37] Lahiri J *et al* 2011 Graphene growth on Ni(111) by transformation of a surface carbide *Nano Lett.* **11** 518–22

[38] Oshima C *et al* 2000 A hetero-epitaxial-double-atomic-layer system of monolayer graphene/monolayer h-BN on Ni(111) *Solid State Commun.* **116** 37–40